Seasonality of phytoplankton cell size and the relation between photosynthesis and respiration in the Ría de Vigo (NW Spain)

J. Lozano[1,*], M. Aranguren-Gassís[1], E. E. García-Martín[1,2], J. González[1], J. L. Herrera[1], B. Hidalgo-Robatto[1], D. Mártinez-Castrillón[1], M. Pérez-Lorenzo[1], R. A. Varela[1], P. Serret[1]

[1]Centro de Investigación Mariña, Universidade de Vigo, Vigo 36310, Spain

[2]Ocean BioGeosciences, National Oceanography Centre, Southampton SO14 3ZH, UK

*Corresponding author: joselozano81@gmail.com

ABSTRACT: The Ría de Vigo is a dynamic and productive upwelling ecosystem. We measured ^{14}C incorporation ($TO^{14}CP$) and gross primary production (GPP), community respiration (DCR), net production (NCP) and size-fractioned chlorophyll *a* (chl *a*) fortnightly from May 2012 to May 2013 in the euphotic layer of the Ría. Our aim was to improve the depiction of plankton metabolism in the Ría and to test the general hypothesis that community structure determines the degree of heterotrophy in planktonic ecosystems. Higher primary production was measured after upwelling episodes and during the spring bloom, when the community was dominated by microphytoplankton (>70% chl $a_{>20\mu m}$). Lower primary production was observed during summer stratification periods (~65% chl $a_{>20\mu m}$), and during the pico- and nanophytoplankton-dominated winter (~25% chl $a_{>20\mu m}$). Coupling between phytoplankton photosynthesis and biomass varied seasonally, mainly driven by environmental conditions. DCR was 3 times lower and 8 times less variable than GPP, and its variability was mainly driven by the changes in chl *a*. The integrated metabolic balance was autotrophic most of the year, despite the negative NCP rates at depth. There was an inverse relationship between the DCR:GPP ratio and the percentage of microphytoplankton (% chl $a_{>20\mu m}$) only in the summer. However, DCR:GPP and DCR:chl *a* ratios were similar in winter

and spring, despite the seasonal differences in primary production and size structure. The similar $TO^{14}CP$:NCP and chl *a*:DCR relations in spring (>70% chl $a_{>20\mu m}$) and winter (~25% chl $a_{>20\mu m}$), and the differences in summer (>70% chl $a_{>20\mu m}$) confirm cell size independence in trophic functioning. We conclude that respiration variability is relevant for the metabolic balance in the Ría, and that the degree of heterotrophy is not systematically related to phytoplankton size over the scales of our study.

KEY WORDS: Upwelling productive system · Plankton metabolism · Community respiration · Primary production · Net community production · Cell size structure · Trophic functioning

1. INTRODUCTION

Eastern boundary upwelling ecosystems (EBUEs) are among the most productive ocean biomes on Earth (Longhurst 2006, Chavez & Messié 2009). They represent approximately 1% of the ocean's surface and contribute around 11% to global new production (Chavez & Toggweiler 1995), supporting >20% of global marine fish catches (Rykaczewski & Checkley 2008). The input of new inorganic nutrients into the euphotic layer by wind-driven advection creates favourable conditions for phytoplankton blooms, typically of large diatoms (Margalef 1978, Falkowski & Oliver 2007), that support simple, efficient food webs (Chavez & Messié 2009 and references therein). The extent, duration and biogeochemical fate of these blooms is determined by the interplay of wind- and density-driven advective and convective currents that control the input of nutrients and the dynamics of particles (Figueiras & Ríos 1993). In addition, the balance between gross primary production (GPP) and the microbial community respiration (DCR), which determines the net community production (NCP, the difference between GPP and DCR), plays a major role in the carbon fate.

The NW Iberian upwelling region (42–44° N) represents the northernmost part of the NW Africa upwelling system (González-Nuevo et al. 2014 and references therein). The upwelling conditions are created by northerly winds that typically last 1–2 wk (Álvarez-Salgado et al. 2000, Gago et al. 2003) and tend to prevail from April to September (Wooster et al. 1976, Álvarez-Salgado et al. 2003). The Ría de Vigo, located in the NW Iberian upwelling region, is a large embayment where upwelling forces a seaward transport of the surface layer that in turn causes the entrance of deep bottom water enriched with inorganic

nutrients and impoverished in oxygen (O_2), creating a positive estuarine circulation in 2 layers (Varela et al. 2005, Crespo et al. 2006). The dynamic circulation created by the upwelling influences the seawater transport between the Ría and the adjacent shelf (Figueiras & Ríos 1993, Álvarez-Salgado et al. 2000), determines its rapid seawater renewal rate (Varela et al. 2005, Herrera et al. 2005) and promotes the offshore export of phytoplankton cells and dissolved organic carbon (Álvarez-Salgado et al. 2003, Gago et al. 2003, Crespo et al. 2006). In contrast, southerly and westerly winds that prevail between October and March create downwelling conditions by promoting the entry of relatively warm and more saline coastal seawater from the surface. Both upwelling and downwelling events occur intermittently throughout the year and are frequently interrupted by phases of thermohaline stratification and vertical mixing. This creates a dynamic hydrographic landscape and a continuous resetting of plankton succession in the Ría de Vigo.

The response of phytoplankton biomass, cell size, species composition and productivity to the upwelling–downwelling cycle in the Ría de Vigo has been previously studied (Margalef 1978, Figueiras & Ríos 1993, Nogueira et al. 1997, Cermeño et al. 2006, Crespo et al. 2006). The rapid changes in hydrographic conditions and plankton community structure have provided empirical evidence to general hypotheses on phytoplankton life-history strategies, succession (Margalef 1978) and trophic dynamics (Cermeño et al. 2006, Arbones et al. 2008). Hence, previous studies showed that metabolic balance is driven by the primary productivity of the system, with DCR representing a minor fraction of the primary production (Moncoiffé et al. 2000) and with NCP depending on phytoplankton cell size structure (Cermeño et al. 2006, Arbones et al. 2008). This latter observation supports the general hypothesis that carbon flows and budgets in pelagic ecosystems depend on phytoplankton cell size (Legendre & Le Fèvre 1989, Kiørboe 1993, Legendre & Rassoulzadegan 1996). According to this hypothesis, food webs of larger organisms (diatoms, metazoan zooplankton) would support relatively minor respiratory rates, leading to autotrophic conditions (NCP > 0) and accumulation of biomass. Conversely, food webs composed of smaller organisms (bacteria, pico-, nanophytoplankton and protists) and characteristic of less optimal growing conditions would increase the degree of heterotrophy (NCP < 0), leading to less sustained biomass (Legendre & Le Fèvre 1989, Kiørboe 1993, Legendre & Rassoulzadegan 1996).

The interpretation of the previous hypothesis assumes that a single and general functional relationship exists between community structure and food web functioning for all

oceanographic conditions, and agrees with the generalised empirical relationship observed between NCP (or the GPP:DCR ratio) and phytoplankton cell size structure (Cermeño et al. 2006, Arbones et al. 2008). However, this observation admits alternative explanations in such a dynamic and heterogeneous landscape, especially when the data sets are mostly from short time scale samplings carried out under distinct oceanographic conditions and with a general prevalence towards upwelling events. Differences in the scale and coupling of trophic and population dynamics and of auto- and heterotrophic processes during different periods (e.g. accumulation or consumption of previously synthesised dissolved organic matter) (e.g. Serret et al. 1999), or the influence on the heterotrophic community of independent variables unrelated to phytoplankton cell size, such as seasonally varying inputs of allochthonous organic matter (e.g. Teira et al. 2009), could bias such a pooled covariation analysis. In this regard, observations of community metabolism at longer/larger scales (based on O_2/argon ratios) (Cassar et al. 2015) and carbon export data (Mouw et al. 2016) have indicated that plankton cell size does not always reliably predict export flux. Therefore, more information on associated changes in food web structure, plankton respiration and net community metabolism is necessary.

Here, we present fortnightly measurements of ^{14}C incorporation ($TO^{14}CP$) and GPP, DCR, NCP and size-fractioned chlorophyll *a* (chl *a*) from May 2012 to May 2013 in the euphotic layer of the Ría de Vigo. To overcome scale difficulties with the empirical relationship between phytoplankton cell size and community metabolism, we examined the relationships between primary production, DCR and NCP during periods with different phytoplankton community composition through the seasonal cycle. Comparison of generalised vs. system-dependent relationships over spatial scales provides robust descriptions of regional changes in food web fluxes (e.g. Serret et al. 2015). The main objectives of this study were to (1) improve the depiction of plankton metabolism seasonality in the Ría de Vigo and the calculation of seasonal and annual metabolic balances in a location representative of the northern part of the NW Africa-Iberian upwelling, and (2) test the general hypothesis that the covariation of phytoplankton cell size structure with NCP implies that community structure determines the degree of heterotrophy of planktonic ecosystems.

2. MATERIALS AND METHODS

2.1. Sampling and hydrographic data

Sampling was carried out fortnightly from 22 May 2012 to 21 May 2013 around pre-dawn at a station in the central channel of the Ría de Vigo (42° 14.07' N, 8° 47.3' W; maximum depth 48 m) (Fig. 1). Water samples from 3, 10 and 20 m depth were collected with 5 l Niskin bottles. Vertical profiles of dissolved O_2 concentration were recorded with a MS5 & DS5X Hydrolab O_2 sensor, calibrated every 2–3 samplings by Winkler measurements of parallel seawater samples collected at each depth. Borosilicate glass bottles (120 ml) were carefully filled from each Niskin bottle using silicon tubing, overflowing the volume of the glass bottle by ca. 1.5 times. Fixing reagents (1 ml of 3 M $MnSO_4$ and 1 ml of 8 M KOH + 4 M KI solution) were added separately with an automatic multi-pipette. Fixing, storage and standardization procedures followed the recommendations of Grasshoff et al. (1983). Measurements of dissolved O_2 were made with an automated Winkler titration system using a Metrohm 848 DMS with a potentiometric end point (Oudot et al. 1988, Pomeroy et al. 1994). O_2 saturation was calculated using the equations for the solubility of oxygen in seawater of Benson & Krause (1984). A vertical profile of photosynthetically active radiation (PAR) was carried out ~2 h after dawn with a Li-Cor sensor. Although we measured our own temperature, conductivity and pressure data with a Seabird 37 CTD probe and also recorded our own vertical profiles of dissolved O_2 with a MS5 & DS5X Hydrolab O_2 sensor, we used instead high-resolution hydrographic and dissolved O_2 data obtained from the INTECMAR webpage (www.intecmar.gal). This high-resolution data was recorded from the same station (from the surface to 30 m deep). Following Varela et al. (2005) and Herrera et al. (2008), representative time series of the upwelling index (UI) computed at the Silleiro Buoy location (42.10° N, 9.39° W) were downloaded from the IEO server (www.ieo .es). Raw UI time series with a 4 d^{-1} sampling frequency, were low-pass filtered using a 1 wk^{-1} cut-off frequency low-pass filter. Both raw and filtered UI time series were daily averaged before being plotted. Rainfall and solar irradiance data from the mouth of the Ría and freshwater inflow data from the Oitavén-Verdugo river were provided by Meteogalicia.

2.2. Inorganic nutrients and chl *a*

Water samples for the determination of inorganic nutrient concentrations were collected directly from each Niskin bottle into 50 ml polystyrene tubes (1 tube per depth), and frozen at –20°C until further analysis. Concentrations of nitrate (NO_3^-), nitrite (NO_2^-), ammonia (NH_4^+), phosphate (PO_4^{3-}) and silicon (Si) were measured following the colorimetric methods described in Grasshoff et al. (1983), using a Skalar San Plus segmented flow autoanalyzer. For chl *a* determination, 250 ml seawater samples (one sample from each

depth) were collected and sequentially filtered through 20, 2 and 0.2 μm pore size polycarbonate filters (Whatman). Filters were immediately frozen at –20°C until further analysis. Chl *a* was extracted from the filters in 90% acetone HPCL at 4°C for 8–17 h in darkness. Fluorescence was measured on a Turner 10-AU fluorometer calibrated against chl *a* standards, following joint global ocean flux study (JGOFS) protocols (Knap et al. 1996).

2.3. Primary production

Seawater samples from each depth were transferred from the Niskin bottle into four 75 ml acid-cleaned polypropylene bottles (3 transparent and 1 dark). Each bottle was inoculated with 50 μCi ml^{-1} $NaH^{14}CO_3$ and then incubated for 24 h in a 1 m depth *in situ* underwater incubator. The incubator was not placed at the sampling location, but near the sampling facility. Bottles were covered with combinations of neutral density plastic meshes to replicate the percentage of surface irradiance (calculated from the PAR readings) from the 3 depths. After the incubation period, seawater samples were filtered at low vacuum (<50 mm Hg) through 0.2 μm polycarbonate filters and the filtrates were collected. The filtrates were acidified with 100–150 μl of 50% HCl, and the filters were fumed with concentrated HCl for 12 h to remove unfixed inorganic ^{14}C (Steemann Nielsen 1952, Peterson 1980). Radioactivity was measured in the filters and filtrates with a β radiation-Wallac scintillation counter to determine total primary production (sum of particulate primary production and dissolved primary production: $TO^{14}CP = PO^{14}CP + DO^{14}CP$).

2.4. Gross primary production, dark community respiration and net community production

In vitro changes in dissolved O_2 concentration were measured after 24 h light and dark bottle incubations at each sampling depth. Twelve 120 ml, gravimetrically calibrated borosilicate glass bottles were carefully filled with seawater which was transferred from each Niskin bottle using silicon tubing, allowing the seawater to overflow. From each depth, 4 pseudo-replicate 'zero' bottles were fixed immediately with 1 ml of 3 M $MnSO_4$ and 1 ml of 8 M KOH + 4 M KI solution. The other 8 bottles were incubated *in situ*: 4 bottles in darkness, wrapped with thick dark coatings ('dark'), and 4 bottles under irradiance conditions simulating those of the original sampling depth ('light'). After 24 h, 'light' and 'dark' bottles were fixed as described in Section 2.3 above.

Measurements of dissolved O_2 were made with an automated Winkler titration system using a Metrohm 848 DMS with a potentiometric end-point (Oudot et al. 1988, Pomeroy et

al. 1994). O_2 metabolic rates (GPP = NCP + DCR) were calculated from the difference between the averages of the pseudo-replicate 'light', 'dark' and 'zero' measurements: NCP = average 'light' [O_2] – average 'zero' [O_2] and DCR = average 'zero' [O_2] – average 'dark' [O_2], where [O_2] is concentration of oxygen. Rates are presented with their standard errors (±SE), calculated as the propagated errors of the average differences.

2.5. Data treatment

Depth- and time-integrated values were obtained by trapezoidal integration of the volumetric or daily data, respectively. The associated SEs of the integrated rates were calculated following the propagation procedure for independent measurements (Miller & Miller 1988). Simple linear regressions (ordinary least squares) were used to analyse the relationships between biological variables. Contour graphs were created using Ocean Data View software (http://odv.awi.de version 4.7.9, 2017). Other graphical and statistical analyses were carried out with Data Graph, RStudio Desktop v.1.3.1093 (R Core Team 2020), and Graph Pad software.

3. RESULTS AND DISCUSSION

3.1. Hydrography

The hydrodynamics of the Ría de Vigo are governed by seasonal thermohaline variability, combined with estuarine circulation and short-term wind-driven upwelling and downwelling episodes, which modify the vertical structure of the water column (Álvarez-Salgado et al. 1993, Varela et al. 2005, Sousa et al. 2011). The inverse annual trends of solar irradiance and freshwater inflow (Fig. S1 in the Supplement at www.int-res.com/articles/suppl/m000p000_supp.pdf) reflect on the annual distribution of seawater density, which shows a characteristic seasonal alternation of stratification and mixing (Fig. 2)

Two main phases of stratification were observed: (1) a period of thermal stratification from mid-May to September 2012, caused by the increasing intensity and duration of daily solar irradiance and characterised by a mean (±SE) vertical (0–35 m depth) temperature gradient of ca. 3.2 ± 1°C; and (2) a period of haline stratification from mid-December 2012 to April 2013 due to intense rain and continental freshwater run-off (Figs. 2 & S1). Both stratification periods were separated by a phase of vertical mixing between October and mid-December 2012. Episodes of wind-driven upwelling modified the vertical structure of the water column by bringing relatively dense seawater towards the surface, evidenced by a

compression of isopycnals in the upper water column. Although the UI was highly variable during the study, 2 distinct periods were discernible: (1) upwelling favourable conditions (positive UI), which prevailed from mid-June to late September 2012, throughout February 2013 and from mid-April to May 2013 (Fig. S1); and (2) downwelling favourable conditions (negative UI), which prevailed between October 2012 and January 2013 as well as during late March and early April 2013 (Fig. S1).

3.2. Dissolved O_2 saturation, NO_3^- and chl *a*

Upwelled seawater masses are generally impoverished in O_2 but rich in inorganic nitrogen (Chavez & Messié 2009) (Fig. 3a,b), although denitrification and anammox in deep anoxic water causes loss of fixed nitrogen to N_2, resulting in a nitrogen deficit compared with remineralised phosphorus (Dalsgaard et al. 2012). High O_2 saturation and high NO_3^- concentration near the surface in winter indicates the biogeochemical impact of continental run-off water accumulated during high precipitation/downwelling episodes (Fig. 3a,b).

There was a temporal variation of chl *a*, with 2 periods of high surface chl *a* in early September and early April 2013 and minimum water column chl *a* in late autumn–winter (November 2012 to mid-February 2013) (Fig. 3c). In addition, surface chl *a* was particularly low during the summer (late May to August 2012) despite the upwelling prevalence in July.

Chl *a* was low near the surface during most of the upwelling–thermal stratification period (Fig. 3c) (late May to October 2012). At the beginning of the sampling in late May 2012, NO_3^- and chl *a* were very low near the surface (<0.5 mol m^{-3} and <1 mg m^{-3}, respectively), while a sub-surface chlorophyll maximum (SCM) of >9 mg m^{-3} was measured above the nitracline at 10 m depth. These results, and the O_2 super-saturation measured near the surface, suggest a surface formation and posterior sedimentation of phytoplankton biomass. The SCM observed at 20 m depth in early July (15 mg m^{-3}) coincided with conditions of both O_2 sub-saturation and relatively high NO_3^- (2.3 mmol m^{-3}) in a phase of upwelling relaxation (Figs. 3 & S1). SCMs are typical in the Ría during periods of relaxation between summer upwelling pulses (e.g. Cermeño et al. 2006, Arbones et al. 2008). We measured very high surface chl *a* and a strong vertical gradient in early September 2012 after an upwelling event that brought an important amount of NO_3^- to the upper layer (>9 mmol m^{-3} at 20 and 10 m depth) (Figs. 2, 3 & S1). This bloom was particularly intense, with volumetric and integrated chl *a* of 21.22 mg m^{-3} and 190.51 mg m^{-2}, which corresponded to almost 2-fold the highest values reported in Cermeño et al. (2006) and Arbones et al. (2008)

(12–13 mg m^{-3} and 129–115 mg m^{-2}). Upwelling conditions returned in late September 2012, after a period of hydrographic relaxation, which drove the increases in O_2 saturation, NO_3^- and chl *a* in early October 2012 (Fig. 3). However, the magnitude of the early October surface bloom was smaller (9.3 mg chl *a* m^{-3}) than the one in early September (Fig. 3c). We named the period between early September and early October 2012 'early autumn'.

Chl *a* remained low through the water column (average 17.84 ± 3.17 mg m^{-2}) during the late autumn–winter period of cooling, mixing and downwelling prevalence (early November 2012 to mid-February 2013) (Figs. 2, 3c & S1). However, these seasonal values were higher than those reported in Cermeño et al. (2006) and Arbones et al. (2008) (winter averages of 8.3 ± 1.4 and 8.25 ± 1.4 mg m^{-2}, respectively). Low chl *a* is expected during the winter due to the combined effect of vertical mixing and reduced irradiance, which restricts the photosynthetic activity of phytoplankton in the euphotic layer (Falkowski 1983). Water column NO_3^- was high (128 ± 12 mmol m^{-2}) during most of the winter.

Chl *a* increased through March, especially in the upper 10 m, reaching 70 mg m^{-2}, close to the 78 mg m^{-2} measured in October 2012. The reduced seasonal haline stratification and the high solar irradiance recorded in March 2013 favoured the initial increase in chl *a* during early spring. However, heavy precipitation during late March 2013 and the prevalence of downwelling caused a strong haline stratification that persisted until mid-April 2013 (Figs. 2 & S1), and very high NO_3^- was found in the surface brackish water (Fig. 3b). In early April 2013, a phytoplankton bloom developed, with chl *a* levels of 12 mg m^{-3} near the surface and a strong vertical gradient. Integrated chl *a* reached 93.9 ± 11.6 mg m^{-2} in early April 2012, similar to the 92.3 ± 51.5 mg m^{-2} measured by Arbones et al. (2008) in April 2004. By early May 2013, and under upwelling relaxation conditions, a SCM had fully developed, with chl *a* concentrations greater than 10 mg m^{-3} at intermediate and deep waters and 6 mg m^{-3} chl *a* near the surface.

3.3. Size-fractioned chl *a*

The seasonal variation of total chl *a* was mainly related to changes in the microphytoplankton (>20 μm) fraction, which was on average around 4 times greater than the nanophytoplankton (2–20 μm) and almost 14 times greater than the picophytoplankton (0.2–2 μm) (Fig. S2). In addition, the nanophytoplankton was approximately 3.5 times more abundant than the picophytoplankton (annual averages of 14.0 ±1.9 vs. 4.0 ± 0.5 mg m^{-2}, respectively).

There was seasonal variability in the contribution of the 3 size-classes to the total chl *a*. Microphytoplankton dominated total chl *a* during the summer thermal stratification and early autumn bloom in 2012 and again during the upwelling period in spring 2013 (with contributions to total chl *a* ranging from 54.8–88.7%). Thus, when total chl *a* exceeded ca. 1 mg m^{-3}, the microphytoplankton fraction tended to dominate the community. In contrast, during late autumn–winter, when total chl *a* was <1 mg m^{-3}, nanoplankton and picoplankton fractions dominated the community (average 50.3 ± 4.0 and 16.5 ± 2.9% of total chl *a*, respectively).

In summary, there was a distinctive seasonal cycle with 3 main phases, as shown in Fig. 4 with 6 biological variables integrated: percentage of the microphytoplankton fraction (% chl $a_{>20\mu m}$), total chl *a*, $TO^{14}CP$, GPP, DCR and NCP. Firstly, during the summer (late May–August 2012) and early autumn (September–October 2012), both DCR and % chl $a_{>20\mu m}$ remained relatively high through the water column, but primary production (GPP and $TO^{14}CP$), NCP, and total chl *a* were more variable in response to the interplay between upwelling and stratification. Secondly, during the late autumn–winter mixing period (November 2012–February 2013), the values of total chl *a*, % chl $a_{>20\mu m}$ as well as those of the metabolic rates were low. Thirdly, during spring 2013 (late February–May 2013) there was a rapid increase in the value of all 6 variables (Fig. 4).

3.4. Photosynthetic ^{14}C incorporation

3.4.1. Spatial and temporal variation of total primary production

We measured $TO^{14}CP$ maximum rates near the surface during the upwelling-related phytoplankton blooms of early autumn 2012 (54.9 ± 3.41 mmol C m^{-3} d^{-1} at 3 m depth), and during the spring bloom 2013 (43.88 ± 3.19 mmol C m^{-3} d^{-1} at 3 m depth) (Fig. 5a). Lower $TO^{14}CP$ rates and weak vertical gradients were observed during the autumn–winter mixing period (0.05 ± 0.002 to 2.34 ± 0.08 mmol C m^{-3} d^{-1}). Overall, the ranges of our volumetric and integrated rates (0.05 ± 0.002 to 72.35 ± 3.31 mmol C m^{-3} d^{-1}, and 6.07 ± 0.8 to 547.54 ± 17 mmol C m^{-2} d^{-1}) were similar to those for particulate primary production recorded by Cermeño et al. (2006) (1.4–68 mmol C m^{-3} d^{-1}, 74–695 mmol C m^{-2} d^{-1}, estimated from short-time ^{14}C incorporation and assuming 10 h of light d^{-1}) and Arbones et al. (2008) (5.2–180 mmol C m^{-2} d^{-1}, estimated from 24 h ^{14}C incorporation) and agree with the general ranges in the Ría de Vigo (4–833 mmol C m^{-2} d^{-1}; Figueiras et al. 2008).

3.4.2. Relation of $TO^{14}CP$ with total chl *a*

The variation of $TO^{14}CP$ matched that of chl *a* (Figs. 5a & 3c), except for the SCM of early July and mid-September. After excluding these outliers with a *z*-score ≥ 2, the general chl *a* to $TO^{14}CP$ relationship was $TO^{14}CP = 3.51(\pm0.18) \times \text{chl } a - 2.28(\pm0.78)$; $R^2 = 0.91$, $p < 0.0001$, $n = 43$.

Hence, chl *a* appears to be a key factor explaining the variation of primary production. The derived general productivity index (PI) (amount of carbon fixed per unit of chl *a*) was, in general, relatively low (ca. 3 mmol C mg^{-1} chl *a* d^{-1}). However, our values would represent net PI, as our ^{14}C incubations lasted 24 h (Marra et al. 2007). Nonetheless, our general PI lies within the PI ranges previously reported in the Ría de Vigo (1.5–10.8 mg C mg^{-1} chl *a* h^{-1} in Cermeño et al. 2006), and within the PI ranges calculated in other upwelling systems such as the Benguela or the Cariaco Basin (Mitchell-Innes & Walker 1991, Muller-Karger et al. 2001, Marra et al. 2007). These studies showed a systematic seasonality related to species succession and environmental conditions. Thus, lower PIs are usually observed in diatom blooms, increasing in value during stratification conditions because of the reduced package effect of small phytoplankton and low nutrient availability (Marra et al. 2007). Our results show that the coupling between photosynthesis and phytoplankton biomass varied seasonally, with a period of minimum productivity during late autumn–winter. Low PI values were calculated during the summer upwelling periods (average 2.11 ± 0.3 mmol C mg^{-1} chl *a* d^{-1}), but also during the late autumn–winter mixing period (1.01 ± 0.40 mmol C mg^{-1} chl *a* d^{-1}) with a community dominated by nano- and picophytoplankton cells (~75%) whose reduced package effect and higher surface-to-volume ratio are supposed to confer higher efficiency (Raven et al. 2005). The PI increased to 4.15 ± 1.23 mmol C mg^{-1} chl *a* d^{-1} during a phase of thermal stratification and dominance of microphytoplankton (64 ± 10%) in June 2012, contrary to previous expectations (Raven et al. 2005, Marra et al. 2007).

3.5. Gross Primary Production

3.5.1. Spatial and temporal variation of GPP

GPP followed seasonal and vertical patterns very similar to those described for $TO^{14}CP$ and total chl *a* (see Figs. 5a,b & 3c). Our ranges of volumetric and integrated GPP (0.11 ± 0.21 to 105.88 ± 0.80 mmol O_2 m^{-3} d^{-1}, and 12.09 ± 4.28 to 848.13 ± 11.41 mmol O_2 m^{-2} d^{-1}) were higher than those reported in Arbones et al. (2008) (ca. <2–80 mmol O_2 m^{-3} d^{-1}, 52.5–462 mmol O_2 m^{-2} d^{-1}) and similar to values reported in Moncoiffé et al. (2000) (<2–

123 mmol O_2 m^{-3} d^{-1}). Assuming a range of photosynthetic quotients of 1.1–1.3, our annual integrated gross production was 709–838 g C m^{-2} yr^{-1}.

3.5.2. Relation of GPP with chl *a* and $TO^{14}CP$

The general linear relationship between total chl *a* and GPP was highly significant, especially when the SCMs were excluded (Fig. 6). The derived general (gross) PI of 5 mmol O_2 mg^{-1} chl *a* d^{-1} was within the range of the slopes of the GPP:chl *a* relationships that Moncoiffé et al. (2000) calculated with surface (7.36 ± 0.63) and with 1% light depth (0.83 ± 0.17) data. A decrease in the gross PI with depth was also observed in our data from the slope of the GPP:chl *a* relationships (Fig. 6): GPP_{3m} = 5.03(±0.21) × chl a_{3m} – 1.47(±1.41), R^2= 0.97, $p < 0.001$, n = 20; GPP_{10m} = 3.11(±0.44) × chl a_{10m} – 1.15(±1.29), R^2= 0.78, $p < 0.001$, n = 16; and GPP_{20m} = 0.66(±0.14) × chl a_{20m} – 0.05(±0.22), R^2= 0.62, p = 0.001, n = 16.

The large difference between the PI at the surface and at 20 m depth (ca. 8 fold) is characteristic of stratified environments (e.g. Mitchell-Innes & Walker 1991, Lorenzo et al. 2004) and indicates adaptation of the phytoplankton to the reduced light at depth (Falkowski 1983). Only during November did the PI_{3m}/PI_{20m} ratio decrease to ca. 1.5, indicating effective mixing of phytoplankton populations, while through the rest of the year the water column mixing seemed to have occurred at slower time scales, allowing phytoplankton cells to adapt to the local light regimes (Falkowski 1983) or enabling the accumulation of allochthonous, ill-adapted phytoplankton at depth. In general, data from the SCMs agreed with the GPP:chl *a* relationship at 20 m depth, and the slope of this relationship was not different with the inclusion of these SCM data points (t = 0.90, df = 31, p = 0.37) (Fig. 6). This suggests that the low PI at 20 m depth is related to the rapid accumulation of ill-adapted large phytoplankters rather than to the physiological adaptation of large cells to progressively darker environments as they sink.

3.6. Net Community Production

The integrated annual DCR (23.8 ± 1.4 mol O_2 m^{-2} yr^{-1}) was approx. 30% of the annual GPP, and this percentage increased to a seasonal maximum of ca. 40% during the winter. Such a relatively low percentage of respiratory consumption implies that the seasonal variability of NCP resembled that of $TO^{14}CP$, GPP and chl *a* (Figs. 3c & 5). NCP maximum rates were measured near the surface both during the upwelling-related phytoplankton blooms of early autumn and in the spring bloom. During the relaxation periods of early July, mid-September and May 2013, NCP rates decreased in relation to the high chl *a* as a

consequence of the increases in DCR. Negative NCP was measured at 20 m throughout most of the year (–1.35 ± 0.40 mmol O_2 m^{-3} d^{-1}) except during the post-bloom period in July (Fig. 5d). In addition, low NCP rates were measured across the water column during the late autumn–winter mixing period (Figs. 4 & 5d). Overall, volumetric NCP rates ranged from –5.67 ± 0.41 mmol O_2 m^{-3} d^{-1} at 20 m depth in early May 2013 to 95.72 ± 0.80 mmol O_2 m^{-3} d^{-1} at 3 m depth in early September (Fig. 5d).

Integrated NCP was negative only twice along the annual series: –5.38 ± 5.11 mmol O_2 m^{-2} d^{-1} in late November, and the annual minimum of –24.66 ± 11.37 mmol O_2 m^{-2} d^{-1} in mid-July (Fig. 4). The highest integrated NCP rate (741.57 ± 11.36 mmol O_2 m^{-2} d^{-1}) was measured, together with the highest $TO^{14}CP$, GPP and chl *a*, during the upwelling-related bloom in early September (Fig. 4). The mean annual integrated NCP was 161.69 ± 44.58 mmol O_2 m^{-2} d^{-1} with a seasonal minimum during the late autumn–winter period (15.1 ± 11.4 mmol O_2 m^{-2} d^{-1}) and a period of similarly low integrated NCP rates during June and July (Fig. 4). Our values were similar to those reported in Arbones et al. (2008): ranges of ca. –10 to 60 mmol O_2 m^{-3} d^{-1} and 25–400 mmol O_2 m^{-2} d^{-1}, annual average of 144 mmol O_2 m^{-2} d^{-1} and winter average of 22.3 mmol O_2 m^{-2} d^{-1}; and similar to those values reported in Moncoiffé et al. (2000): ca. –18 to 110 mmol O_2 m^{-3} d^{-1} and annual NCP average of 140 mmol O_2 m^{-2} d^{-1}.

Assuming an oxygen to carbon (O_2:C) stoichiometry of 215/147 (Pérez et al. 2000), our annual integrated NCP would result in a net annual production of organic carbon in the Ría de Vigo of 427 ± 20 g C m^{-2} yr^{-1}. This result is significantly higher than the 317 ± 13 g C m^{-2} yr^{-1} estimated by Alonso-Pérez et al. (2015) from the results in Arbones et al. (2008), and higher than the 306 g C m^{-2} yr^{-1} estimated from nitrogen mass balances in the nearby Ría de Arousa by Álvarez-Salgado et al. (2010).

3.7. Dark Community Respiration

3.7.1. Spatial and temporal variation of DCR

Compared to $TO^{14}CP$ and GPP, DCR was lower in both magnitude and variability. The average volumetric and integrated DCR rates were approximately 3 times smaller than the corresponding GPP rates, and DCR annual ranges were 8 and 6 times smaller than those reported of volumetric and integrated GPP, respectively (Figs. 4 & 5). Our DCR rates (0.41 ± 0.10 to 13.32 ± 0.47 mmol O_2 m^{-3} d^{-1} and 15.18 ± 2.01 to 148.88 ± 5.26 mmol O_2 m^{-2} d^{-1})

were similar to those reported in Moncoiffé et al. (2000) (<1–46 mmol O_2 m^{-3} d^{-1}) and Arbones et al. (2008) (<2–20 mmol O_2 m^{-3} d^{-1}; 31–132 mmol O_2 m^{-2} d^{-1}).

High DCR rates were measured during the summer and in the spring bloom (Fig. 5c). Contrary to $TO^{14}CP$ and GPP, high DCR (>7 mmol O_2 m^{-3} d^{-1}) was measured not only near the surface but also at depth, especially during upwelling relaxation periods. Lower DCR rates were observed throughout the water column during the late autumn–winter period (0.86 ± 0.09 mmol O_2 m^{-3} d^{-1}) (Fig. 5c), and DCR rates remained low during early spring (avg. of 1.68 ± 0.21 mmol O_2 m^{-3} d^{-1} from late February to late March). Average DCR/chl *a* was 1.29 ± 0.24 in the spring, similar to late autumn–winter mean of 1.20 ± 0.19 mmol O_2 mg^{-1} chl *a* d^{-1}, and almost half the average measured during summer: 2.35 ± 0.38 mmol O_2 mg^{-1} chl *a* d^{-1}. It is worth noting that the relationship of temperature with DCR was not significant.

Integrated DCR was very low during late autumn and winter (avg. 17.13 ± 0.66 mmol O_2 m^{-2} d^{-1}), and increased steadily during the spring, following the increase of chl *a*. However, integrated DCR remained high during summer (avg. 107.56 ± 10.26 mmol O_2 m^{-2} d^{-1}), lagging behind during phases of decreasing GPP and chl *a* (e.g. mid-July, mid-September), and not showing any significant increase during the phytoplankton bloom in early September (Fig. 4).

3.7.2. Relation of DCR with chl *a* and GPP

The patterns described above indicate a poor correlation between integrated DCR and either chl *a* or GPP during the summer (late May–August 2012) (Fig. 7). In addition, the late autumn–winter integrated data fit well with the significant relationships for the spring period (late February–May 2013) (Fig. 7): DCR = 0.67(±0.10) × chl *a* + 6.50(±10.81), R^2 = 0.89, p <0.001, n = 7 and DCR = 0.12(±0.04) × GPP + 21.01(±8.45), R^2 = 0.81, p <0.001, n = 5. The early autumn (September–October 2012) integrated data also conformed to the relationships for the spring period, implying that the simple variation in total chl *a* explains a major part of the DCR variation in the Ría de Vigo during most of the year except for summer (Fig. 7b). The pooled 'September 2012 to late May 2013' equation is DCR = 0.62(±0.05) × chl *a* + 8.43(±5.30), R^2 = 0.91, p < 0.0001 n = 14. Data points from early autumn 2012 and May 2013 behave as outliers in the DCR:GPP relationship, however they are a good fit in chl *a*:DCR (Fig. 7). These observations indicate a tighter coupling of DCR with chl *a* than with primary production ($TO^{14}CP$ and GPP) in the Ría de Vigo, possibly due to differences in their timescale of variation. Both chl *a* and autotrophic respiration are closely connected to

phytoplankton biomass, and hence with photosynthesis, when the system is in steady state. On the other hand, heterotrophic respiration is logically more connected to the availability of organic substrates to oxidize rather than to their production by photosynthesis. This implies that in a non-steady-state scenario, any instantaneous GPP measurement may not be representative of accumulated biomass. Likewise, in such a non-steady-state scenario, a similar scale of variation for chl *a* and DCR and a different one for GPP could be expected. This would explain why some SCM data points are outliers in the relationships between the less coupled variables (chl *a*:GPP and GPP:DCR) (Figs. 6 & 7a), and inliers in the relationships between the more coupled variables (chl *a*:DCR and $TO^{14}CP$:GPP) (Figs. 7b & 8). This agrees with the uncoupling of phytoplankton biomass and net metabolism size distributions observed by Soria-Píriz et al. (2017) over spatial scales along a tropical estuarine gradient. In highly dynamic and spatially heterogeneous ecosystems like the Ría de Vigo, where the coupling of photosynthesis and biomass varies over short time scales (see Sections 3.4.2 and 3.5.2 above), integrative slow variables such as chl *a* or DCR may more accurately capture the overall productivity and functioning of the system (Carpenter & Turner 2001), while fast variables such as photosynthesis ($TO^{14}CP$ and GPP) would require a strict matching of sampling and forcing scales.

3.7.3. Relationship of DCR with percentage of microphytoplankton (% chl $a_{>20\mu m}$)

The observations described above seem at odds with the hypothesis that the variability of community metabolism in the Ría de Vigo is dependent on phytoplankton cell size structure. This hypothesis is based on the idea that any increase in the dominance of the phytoplankton community by small cells leads to an enhancement of organic matter remineralisation through the microbial food web, thus increasing the relative importance of respiration, whereas whenever large phytoplankton dominates the community, a classical, short food web will prevail, thus reducing organic matter remineralisation and respiration (Cermeño et al. 2006, Arbones et al. 2008 and references therein). We observed higher DCR rates per unit of chl *a* or GPP in the microphytoplankton-dominated summer than during the rest of the year (Figs. 4 & 7). Moreover, the relationship between % chl $a_{>20\mu m}$ and DCR (Fig. 9a) confirms that our observations do not fully concur with this hypothesis. Firstly, higher DCR rates were obtained with higher dominance of the microphytoplankton, suggesting that a third factor, possibly chl *a* or GPP, is underlying the % chl $a_{>20\mu m}$ to DCR relation. The fact that DCR remained low in late autumn (November) and especially during the winter–spring transition (late February), when low chl *a* and low GPP coincided with relatively high % chl

$a_{>20\mu m}$ (Fig. 4) further support the poor response of the heterotrophic metabolism to unique changes in phytoplankton size structure. The relationships of % chl $a_{>20\mu m}$ with the DCR/chl *a* and the DCR:GPP ratios confirm this conclusion: the negative slopes that conform to the hypothesis above were only observed within the summer subset of the data (Fig. 9b, c). However, the DCR:chl *a* and DCR:GPP ratios for the spring period varied little over a range of % chl $a_{>20\mu m}$ similar to the corresponding summer range (ca. 50–90%). Moreover, these ratios were similar in the late autumn–winter and spring across the whole annual range of % chl $a_{>20\ \mu m}$ (<30% in late autumn–winter to >0% in spring) (Fig. 9b,c).

3.8. Phytoplankton size structure and community metabolism

The hypothesis that the metabolic balance in the Ría de Vigo depends on phytoplankton cell size structure is based upon theoretical predictions (Legendre & Le Fèvre 1989, Kiørboe 1993, Legendre & Rassoulzadegan 1996) and the observation of a higher percentage of primary production consumed by community respiration during winter, when small phytoplankton prevail, than during summer stratification and upwelling conditions (Cermeño et al. 2006). According to the same hypothesis, the microbial food web is actively sustained throughout the year by a background level of small phytoplankton and dissolved organic carbon production. Whenever the relative contribution of large-sized phytoplankton increases during the upwelling-favourable season, a higher amount of organic carbon circulates through the classical food web, leading to an increase in the photosynthesis-to-respiration ratio.

Arbones et al. (2008) also obtained positive relationships between the GPP/DCR ratio and % chl $a_{>20\mu m}$ and % $PO^{14}CP_{>20\mu m}$, finding a high degree of autotrophy when large-size phytoplankton were dominant, whereas the system was almost in balance when small phytoplankton prevailed (Fig. 10). Our data show a similar general trend between the GPP:DCR ratio and % chl $a_{>20\mu m}$ as was found by Arbones et al. (2008) (Fig. 10). Similarly, we observed low GPP:DCR ratios during the winter, when pico- and nanophytoplankton represented >70%, and higher ratios in some summer and spring data. An analysis based on comparison of seasonal averages (e.g. Cermeño et al. 2006) would indicate higher autotrophy in the microplankton-dominated summer period. However, both our trend and the one in Arbones et al. (2008) conceal some variability that is not consistent with the hypothesis above.

The relationships found by Arbones et al. (2008) were only sustained when the whole set of data from 5 short-term, high-resolution samplings were analysed. However, the GPP/DCR ratio remained essentially invariant around 2 during the surveys of January and April, even with % chl $a_{>20\mu m}$ and % $PO^{14}CP_{>20\mu m}$ ranging from <20 to >90% (Fig. 10). This ratio increased to 6.2 only in July, despite % chl $a_{>20\mu m}$ and % $PO^{14}CP_{>20\mu m}$ (85 and 91%, respectively) being very similar to those in April and October (88–92 and 79–83%, respectively). Similarly, in our study the GPP:DCR ratio remained around 2 during most of the year (late autumn, winter, most spring and some summer data), despite % chl $a_{>20\mu m}$ ranging from <20 to >90% (Fig. 10). We measured low NCP rates and GPP:DCR ratios throughout the summer, when % chl $a_{>20\mu m}$ was 65 ± 5% (Figs. 4, 5 & 10). Moreover, we measured the only significant negative NCP value during the microphytoplankton-dominated summer. These observations are in agreement with our relationship between % chl $a_{>20\ \mu m}$ and the DCR:chl *a* ratio (Fig. 9c), confirming that a more stringent test is necessary to decipher the dependence of trophic balances upon phytoplankton cell size structure.

The variation in the relationship between primary production and DCR or NCP has been used to identify differences in the trophic functioning between distinct ecosystems (Serret et al. 2015 and references therein) and hence opens a potential for testing the hypothesis above. According to this hypothesis, during the winter, with small cells dominating an unproductive phytoplankton community, the higher degree of heterotrophy should cause the slope of the $TO^{14}CP$:NCP relationship to be lower than during the spring and summer. However, in our study, the relationships between $TO^{14}CP$ and NCP (Fig. 11) as well as the variation of DCR with chl *a* and GPP (Fig. 7) all indicate similar trophic functioning during the late autumn–winter period (dominated by pico- and nanophytoplankton) and during the spring and early autumn periods (both dominated by microphytoplankton); while the trophic functioning during the summer period (dominated by microphytoplankton) was different. The significant $TO^{14}CP$:NCP relationship for early autumn, winter and spring shows an intercept that is not significantly different from zero and a lower slope than the summer relationship, whose intercept is negative (Fig. 11). With similar levels of high % chl $a_{>20\mu m}$ in the summer and spring (Figs. 4 & S2), these relationships show that at high levels of productivity (GPP > 300 mmol O_2 m^{-2} d^{-1}), there is a marginal tendency towards a higher degree of autotrophy in the summer than in the spring (mean GPP:DCR ratios of 6.4 ± 3.8 and 4.9 ± 1.12, respectively). However, as the productivity decreases (GPP < 200 mmol O_2 m^{-2} d^{-1}), the degree of heterotrophy increases

more in summer than in spring (Fig. 11), irrespective of the prevailing phytoplankton size (mean GPP/DCR ratios of 1.3 ± 0.2 in summer [n = 5] and 3.3 ± 0.15 in spring [n = 3]; Fig. 7a). Additionally, below a GPP of 200 mmol O_2 m^{-2} d^{-1}, the degree of heterotrophy is even higher in the summer, with >70% chl $a_{>20\mu m}$, than in the late autumn–winter period, with <30% chl $a_{>20\mu m}$ (the average GPP/DCR ratio would be 1.3 ± 0.2 in summer [n = 5] and 1.9 ± 0.6 in late autumn–winter [n = 3]; Fig. 7a). For further consistency, a very similar size-independent seasonality in the degree of heterotrophy is observed when DCR is related to total chl *a* and % chl $a_{>20\mu m}$ (Figs. 7 & 9).

Our results imply that phytoplankton cell size does not determine the seasonal variability in the degree of heterotrophy in the Ría de Vigo. It is logical that community respiration should be higher per unit of biomass or per unit of production in a complex microbial food web where heterotrophic activities play key roles than in a simpler, 'classical' food web (Legendre & Le Fèvre 1989, Kiørboe 1993, Legendre & Rassoulzadegan 1996). Additionally, large heterotrophs were poorly represented in the 120 ml O_2 incubation bottles. However, is not necessarily correct that any change in phytoplankton cell size should immediately trigger a shift in the prevailing route of organic matter circulation across the continuum between the 2 types of food webs mentioned. This is especially true when the prevalence of small cells occurs in low-light and high-nutrient, turbulent environments (e.g. the winter in the Ría de Vigo) rather than in oligotrophic, stratified systems where nutrient remineralisation is essential. Processes that may interrupt the functional connection between community structure and food web fluxes include the consumption of previously accumulated or allochthonous organic matter, bioavailability of inorganic and organic matter for heterotrophs or size-selective grazing (Teira et al. 2009, Cassar et al. 2015, Mouw et al. 2016). As a result, communities with similar phytoplankton cell size structure may show different trophic functioning in highly episodic systems punctuated by inputs of deep NO_3^- (e.g. during summer) than during seasonal transitions that are characterized by runoff and inputs of allochthonous reduced inorganic and organic nitrogen (e.g. spring).

Our observations contradict the hypothesis that planktonic carbon flows and budgets in the Ría de Vigo are dependent on phytoplankton size structure (Cermeño et al. 2006, Arbones et al. 2008). This conclusion is supported by observations of high NCP in communities dominated by nano- and picoplankton in the Southern Ocean (Cassar et al. 2015) or tropical estuaries (Soria-Píriz et al. 2017). The theoretical expectations are met when extreme situations are compared, e.g. the highly autotrophic microphytoplankton-dominated

upwelling and spring phytoplankton blooms vs. the almost in balance pico- and nanophytoplankton-dominated winter mixing (e.g. Fig. 10, see also Cermeño et al. 2006, Arbones et al. 2008), or during rapid successions within the highly transient summer period (Fig. 9). However, the metabolic balance is not dependent on phytoplankton size structure over the range of ecological states observed throughout the year, particularly at intermediate productivity regimes and during seasonal transitions.

Generalised $TO^{14}CP$:NCP models, even adjusted to changes in phytoplankton cell size, are not sufficient to accurately predict annual net community metabolism, which requires a sound representation of the seasonal variability in the relationship between photosynthesis and respiration. For example, our summer $TO^{14}CP$:NCP relationship would incorrectly predict consistent net heterotrophy through the late autumn–winter period (–64.49 ± 5.99 mmol O_2 m^{-2} d^{-1}), while the pooled autumn–winter–spring model would overestimate NCP during low-productivity periods in the summer. The impact of these biases in the Ría de Vigo may be relatively minor because of the high contribution of phytoplankton blooms to the annual NCP and the general prevalence of autotrophy throughout the year. The generalized $TO^{14}CP$:NCP model would underestimate the winter NCP by 6.8 mol O_2 m^{-2}. Accurate prediction of changes in NCP under foreseeable scenarios of climate-induced changes in upwelling intensity and a general increase in continental runoff will require understanding of the variability and processes controlling respiration rates, as well as deciphering the scaling of primary production and community respiration in EBUEs.

Acknowledgements. We thank the ECIMAT coastal station of the Universidad de Vigo for technical support with the incubations and sample processing. This research was funded by the Spanish MICINN grant CTM2011-29616 (SCALAR) awarded to P.S. J.L. was funded by a MICINN FPI fellowship. We thank the Unidad de Muestreo Oceanográfico del Servicio Científico Técnico de la Universidad de Oviedo for the analyses of nutrients.

LITERATURE CITED

Alonso-Pérez F, Zúñiga D, Arbones B, Figueiras FG, Castro CG (2015) Benthic fluxes, net ecosystem metabolism and seafood harvest: completing the organic carbon balance in the Ría de Vigo (NW Spain). Estuar Coast Shelf Sci 163:54–63 doi:10.1016/j.ecss.2015.05.038

Álvarez-Salgado XA, Rosón G, Pérez FF, Pazos Y (1993) Hydrographic variability off the Rías Baixas (NW Spain) during the upwelling season. J Geophys Res 98:14447–14455 doi:10.1029/93JC00458

Álvarez-Salgado XA, Gago J, Míguez BM, Gilcoto M, Pérez FF (2000) Surface waters of the NW Iberian margin: upwelling on the shelf versus outwelling of upwelled waters from the Rías Baixas. Estuar Coast Shelf Sci 51:821–837 doi:10.1006/ecss.2000.0714

Álvarez-Salgado XA, Figueiras FG, Pérez FF, Groom S and others (2003) The Portugal coastal counter current off NW Spain: new insights on its biogeochemical variability. Prog Oceanogr 56:281–321 doi:10.1016/S0079-6611(03)00007-7

Álvarez-Salgado XA, Vieira Borges A, Figueiras FG, Chou L (2010) Iberian margin: the Rías. In: Liu KK, Atkinson L, Quiñones R, Talaue-McManus L (eds) Carbon and nutrient fluxes in continental margins. Springer-Verlag, Berlin, p 103–120

Arbones B, Castro CG, Alonso-Perez F, Figueiras FG (2008) Phytoplankton size structure and water column metabolic balance in a coastal upwelling system: the Ría de Vigo, NW Iberia. Aquat Microb Ecol 50:169–179 doi:10.3354/ame01160

Benson BB, Krause D Jr (1984) The concentration and isotopic fractionation of oxygen dissolved in freshwater and seawater in equilibrium with the atmosphere. Limnol Oceanogr 29:620–632 doi:10.4319/lo.1984.29.3.0620

Carpenter SR, Turner MG (2001) Hares and tortoises: interactions of fast and slow variables in ecosystems. Ecosystems 3:495–497 doi:10.1007/s100210000043

Cassar N, Wright SW, Thompson PG, Trull TW and others (2015) The relation of mixed-layer net community production to phytoplankton community composition in the Southern Ocean. Global Biogeochem Cycles 29:446–462 doi:10.1002/2014GB004936

Cermeño P, Marañón E, Pérez V, Serret P, Fernández E, Castro CG (2006) Phytoplankton size structure and primary production in a highly dynamic coastal ecosystem (Ría de Vigo, NW-Spain): seasonal and short-time scale variability. Estuar Coast Shelf Sci 67:251–266 doi:10.1016/j.ecss.2005.11.027

Chavez FP, Messié M (2009) A comparison of eastern boundary upwelling ecosystems. Prog Oceanogr 83:80–96 doi:10.1016/j.pocean.2009.07.032

Chavez FP, Toggweiler JR (1995) Physical estimates of global new production: the upwelling contribution. In: Summerhayes CP, Emeis KC, Angel MV, Smith RL, Zeitzschel B

(eds) Dahlem workshop on upwelling in the ocean: modern processes and ancient records. John Wiley & Sons, Chichester, p 313–320

Crespo BG, Figueiras FG, Porras P, Teixeira IG (2006) Downwelling and dominance of allochthonous dinoflagellates in the NW Iberian margin: the example of the Ría de Vigo. Harmful Algae 5:770–781 https://doi.org/10.1016/j.hal.2006.03.006

Dalsgaard T, Thamdrup B, Farías L, Revsbech NP (2012) Anammox and denitrification in the oxygen minimum zone of the eastern South Pacific. Limnol Oceanogr 57:1331–1346 doi:10.4319/lo.2012.57.5.1331

Falkowski PG (1983) Light-shade adaptation and vertical mixing of marine phytoplankton: a comparative field study. J Mar Res 41:215–237 doi:10.1357/002224083788520199

Falkowski PG, Oliver MJ (2007) Mix and match: how climate selects phytoplankton. Nat Rev Microbiol 5:813–819 PubMed doi:10.1038/nrmicro1751

Figueiras FG, Ríos AF (1993) Phytoplankton succession, red tides and the hydrographic regime in the Rías Bajas of Galicia. In: Smayda TJ, Shimizu Y (eds) Toxic phytoplankton blooms in the sea. Elsevier, New York, NY p 239–244>

Figueiras FG, Miranda A, Riveiro I, Vergara AR, Guisande C (2008) El plankton de la Ría de Vigo. In: González-Garcés Santiso A, Vilas Martín F, Álvarez-Salgado XA (eds) La Ría de Vigo: una aproximación integral al ecosistema marino de la Ría de Vigo. Instituto de Estudios Vigueses, Vigo, p 111–152

Gago J, Gilcoto M, Pérez FF, Ríos AF (2003) Short-term variability of CO2 in seawater and air–sea CO2 fluxes in a coastal upwelling system (Ría de Vigo, NW Spain). Mar Chem 80:247–264 doi:10.1016/S0304-4203(02)00117-2

González-Nuevo G, Gago J, Cabanas JM (2014) Upwelling index: a powerful tool for marine research in the NW Iberian upwelling system. J Oper Oceanogr 7:47–57https://doi.org/10.1080/1755876X.2014.11020152

Grasshoff K, Erhardt M, Kremlin M (1983) Methods of seawater analysis, 2nd edn. Verlag Chemie, Weinheim

Herrera JL, Piedracoba S, Varela RA, Rosón G (2005) Spatial analysis of the wind field on the western coast of Galicia (NW Spain) from in situ measurements. Cont Shelf Res 25:1728–1748 doi:10.1016/j.csr.2005.06.001

669 Herrera JL, Rosón G, Varela RA, Piedracoba S (2008) Variability of western Galician
670 upwelling system (NW Spain) during an intensively sampled annual cycle. An EOF analysis
671 approach. J Mar Sys 72:200–217 doi:10.1016/j.jmarsys.2007.07.007

672 Kiørboe T (1993) Turbulence, phytoplankton cell size and the structure of pelagic
673 food webs. Adv Mar Biol 29:1–72 doi:10.1016/S0065-2881(08)60129-7

674 Knap AH, Michaels AE, Close A, Ducklow HW, Dickson AG (eds) (1996) Protocols
675 for the joint global ocean flux study (JGOFS) core measurements. JGOFS Report No 19.
676 UNESCO, Bergen

677 Legendre L, Le Fèvre J (1989) Hydrodynamical singularities as controls of recycled
678 versus export production in oceans. In: Berger WH, Smetacek VS, Wefer G (eds)
679 Productivity of the oceans: present and past. John Wiley & Sons, Hoboken, NJ, p 49–63

680 Legendre L, Rassoulzadegan F (1996) Food-web mediated export of biogenic carbon
681 in oceans: environmental control. Mar Ecol Prog Ser 145:179–193 doi:10.3354/meps145179

682 Longhurst A (2006) Ecological geography of the sea. Academic Press, New York,
683 NY

684 Lorenzo L, Figueiras FG, Tilstone GH, Arbones B, Mirón I (2004) Photosynthesis
685 and light regime in the Azores Front region during summer: Are light-saturated computations
686 of primary production sufficient? Deep Sea Res I 51:1229–1244
687 doi:10.1016/j.dsr.2004.01.010

688 Margalef R (1978) What is an upwelling ecosystem? In: Boje R, Tomczak M (eds)
689 Upwelling ecosystems. Springer, Berlin, p 12–14

690 Marra J, Trees CC, O'Reilly JE (2007) Phytoplankton pigment absorption: a strong
691 predictor of primary productivity in the surface ocean. Deep Sea Res I 54:155–163
692 doi:10.1016/j.dsr.2006.12.001

693 Miller JC, Miller JN (1988) Statistics for analytical chemistry, 2nd edn. Ellis
694 Horwood, Chichester

695 Mitchell-Innes BA, Walker DR (1991) Short-term variability during an anchor station
696 study in the southern Benguela upwelling system: phytoplankton production and biomass in
697 relation to species changes. Prog Oceanogr 28:65–89 doi:10.1016/0079-6611(91)90021-D

Moncoiffé G, Álvarez-Salgado XA, Figueiras FG, Savidge G (2000) Seasonal and short-time-scale dynamics of microplankton community production and respiration in an inshore upwelling system. Mar Ecol Prog Ser 196:111–126 doi:10.3354/meps196111

Mouw CB, Barnett A, McKinley GA, Gloege L, Pilcher D (2016) Phytoplankton size impact on export flux in the global ocean. Global Biogeochem Cycles 30:1542–1562https://doi.org/10.1002/2015GB005355

Muller-Karger F, Varela R, Thunell R, Scranton M and others (2001) Annual cycle of primary production in the Cariaco Basin: response to upwelling and implications for vertical export. J Geophys Res 106:4527–4542https://doi.org/10.1029/1999JC000291

Nogueira E, Pérez FF, Ríos A (1997) Seasonal patterns and long-term trends in an estuarine upwelling ecosystem (Ría de Vigo, NW Spain). Estuar Coast Shelf Sci 44:285–300 doi:10.1006/ecss.1996.0119

Oudot C, Gerard R, Morin P, Gningue I (1988) Precise shipboard determination of dissolved oxygen (Winkler procedure) for productivity studies with a commercial system. Limnol Oceanogr 33:146–150 doi:10.4319/lo.1988.33.1.0146

Pérez FF, Álvarez–Salgado XA, Rosón G (2000) Stoichiometry of nutrients (C, N, P and Si) consumption and organic matter production in a coastal inlet affected by upwelling. Mar Chem 69:217–236 doi:10.1016/S0304-4203(99)00107-3

Peterson BJ (1980) Aquatic primary productivity and the 14C-CO2 method: a history of the productivity problem. Ann Rev Ecol Syst 11:359–385 //doi.org/10.1146/annurev.es.11.110180.002043

Pomeroy LR, Sheldon JE, Sheldon WM Jr (1994) Changes in bacterial numbers and leucine assimilation during estimations of microbial respiratory rates in seawater by the precision Winkler method. Appl Environ Microbiol 60:328–332 PubMed doi:10.1128/AEM.60.1.328-332.1994

R Core Team (2020) R: a language and environment for statistical computing. R Foundation for Statistical Computing,

Raven JA, Finkel ZV, Irwin AJ (2005) Picophytoplankton: bottom-up and top-down controls on ecology and evolution. Vie Milieu 55:209–215

Rykaczewski RR, Checkley DM Jr (2008) Influence of ocean winds on the pelagic ecosystem in upwelling regions. Proc Natl Acad Sci USA 105:1965–1970 PubMed doi:10.1073/pnas.0711777105

Serret P, Fernández E, Sostres JA, Anadón R (1999) Seasonal compensation of microbial production and respiration in a temperate sea. Mar Ecol Prog Ser 187:43–57 doi:10.3354/meps187043

Serret P, Robinson C, Aranguren-Gassís M, García-Martín EE and others (2015) Both respiration and photosynthesis determine the scaling of plankton metabolism in the oligotrophic ocean. Nat Commun 6:6961 PubMed doi:10.1038/ncomms7961

Soria-Píriz S, García-Robledo E, Papaspyrou S, Aguilar V and others (2017) Size fractionated phytoplankton biomass and net metabolism along a tropical estuarine gradient. Limnol Oceanogr 62:S309–S326 doi:10.1002/lno.10562

Sousa MC, Alvarez I, Vaz N, Dias JM (2011) Physical forcing of the hydrography of the Ria de Vigo mouth. J Coast Res 64:1589–1593

Steemann Nielsen E (1952) The use of radio-active carbon (C14) for measuring organic production in the sea. J Mar Sci 18:117–140

Teira E, Martínez-García S, Lønborg C, Álvarez-Salgado XA (2009) Growth rates of different phylogenetic bacterioplankton groups in a coastal upwelling system. Environ Microbiol Rep 1:545–554 PubMed doi:10.1111/j.1758-2229.2009.00079.x

Varela RA, Rosón G, Herrera JL, Torres-López S, Fernández-Romero A (2005) A general view of the hydrographic and dynamical patterns of the Rías Baixas adjacent sea area. J Mar Syst 54:97–113 doi:10.1016/j.jmarsys.2004.07.006

Wooster WS, Bakun A, McClain DR (1976) The seasonal upwelling cycle along the eastern boundary of the North Atlantic. J Mar Res 34:131–141

FIGURES

Fig. 1. Sampling station at the Ría de Vigo. Modified from Cermeño et al. (2006)

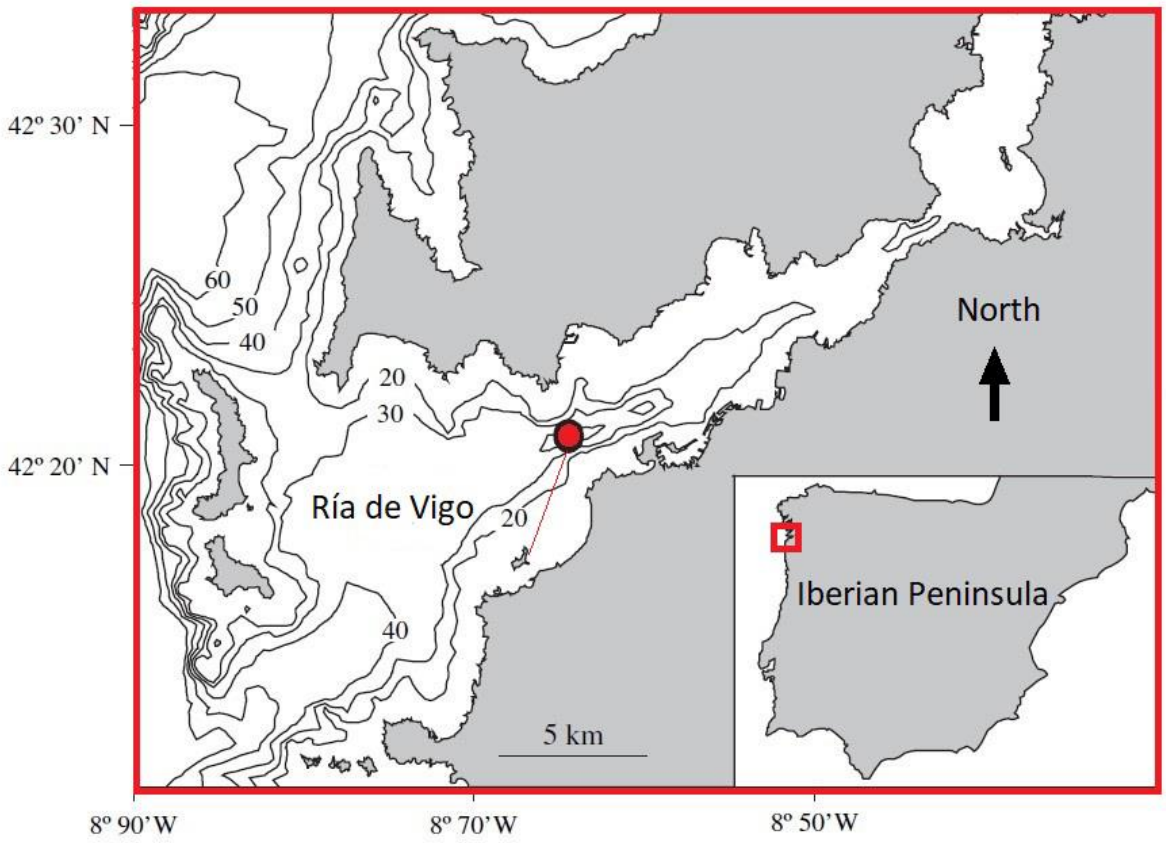
42º 30' N
42º 20' N
8º 90'W
8º 70'W
8º 50'W
60
50
40
20
30
20
40
Ría de Vigo
North
Iberian Peninsula
5 km

754

Fig. 2. Vertical and temporal variability of (a) temperature, (b) salinity and (c) density of seawater at the sampling station in the Ría de Vigo during the period of study. Black dots: position of *in situ* seawater sampling points for chemical and biological variables

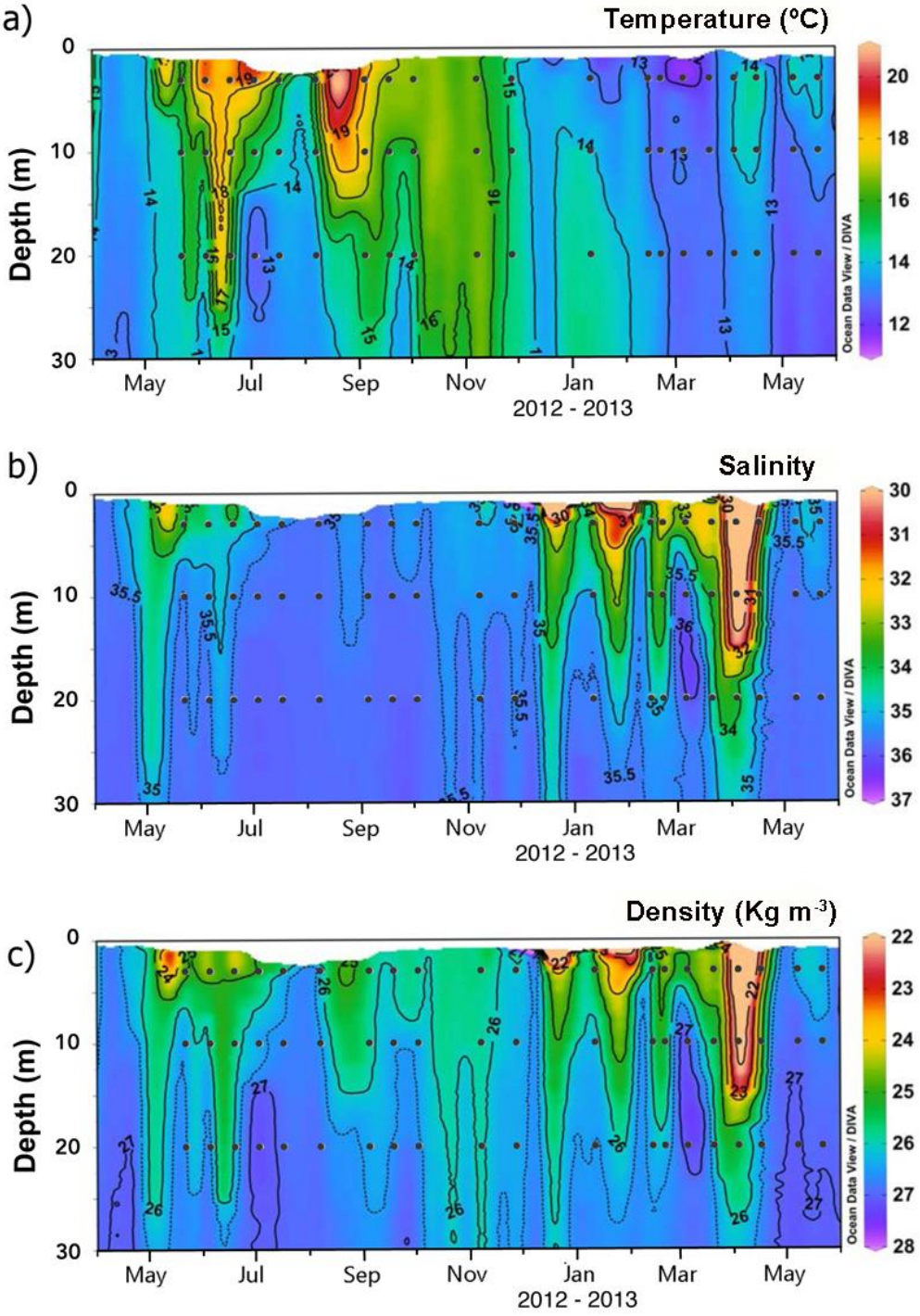

Fig. 3. Vertical and temporal variation of (a) percentage of oxygen saturation, (b) nitrate and (c) total chlorophyll *a* (chl *a*) in the Ría de Vigo. In (c), the key oceanographic situations and ecological transitions described in the text are indicated approximately (white diamonds: sub-surface chlorophyll maximums, SCMs). Note that the spatial and temporal resolution and extent of oxygen measurements from the Iberian Shelf Oceanographic Observatory are higher than those of the seawater sampling for nitrate and total chl *a* (black dots)

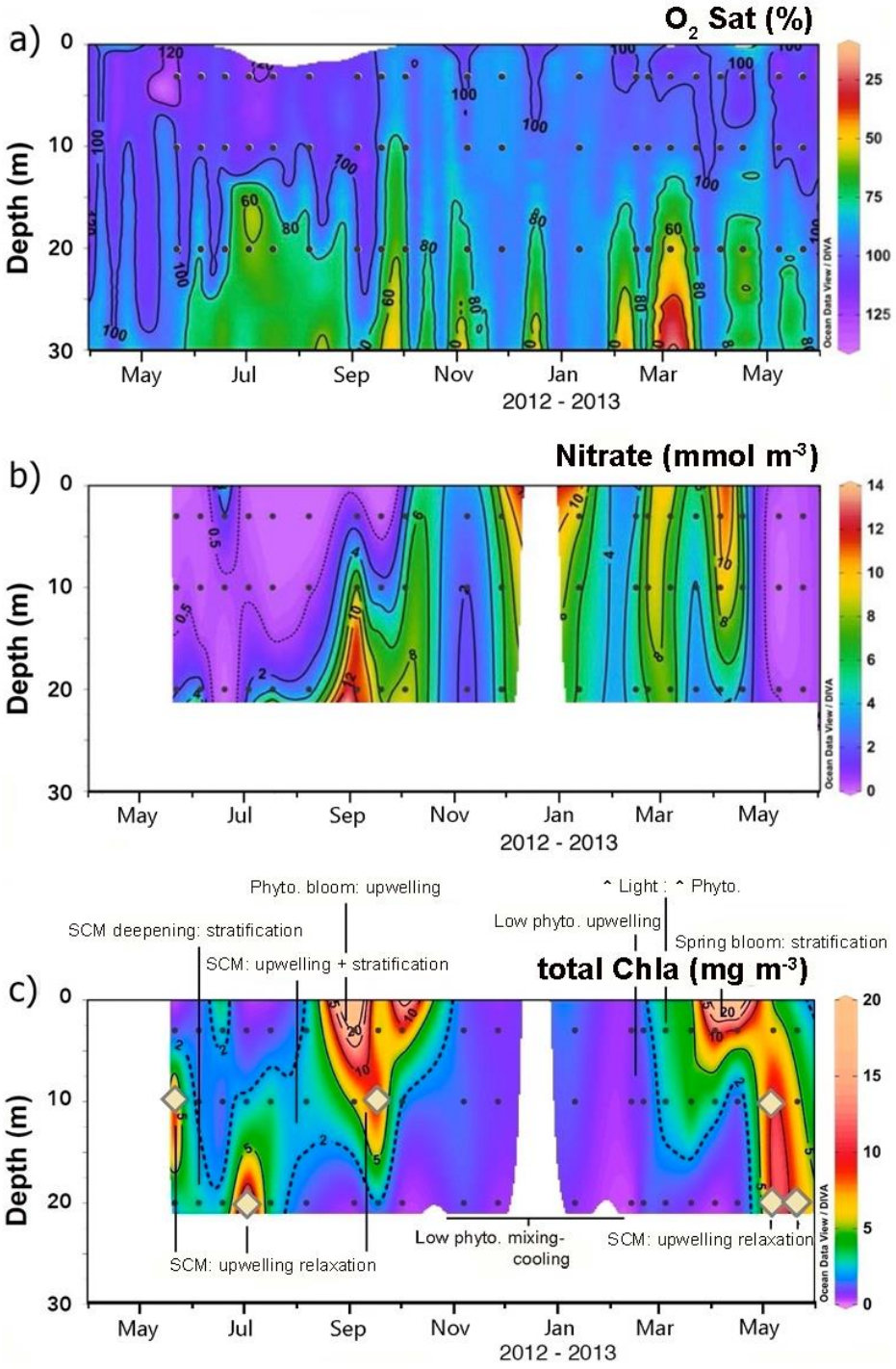

768 Fig. 4. Temporal variation of integrated percentage of microphytoplankton (% chl
769 $a_{>20\mu m}$), total chl *a* and integrated metabolic rates: total photosynthetic ^{14}C incorporation
770 ($TO^{14}CP$), gross primary production (GPP), net community production (NCP) and
771 community respiration (DCR) measured at the sampling station in the Ría de Vigo. Error
772 bars: corresponding propagated SE; dashed line: zero NCP

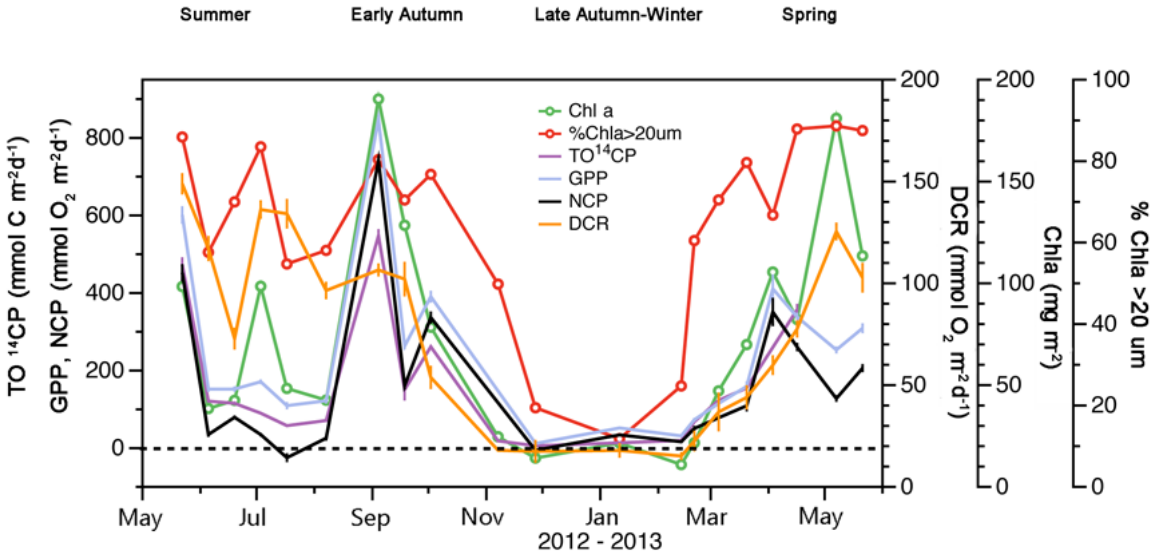

773

774

Fig. 5. Vertical and temporal variation of (a) total photosynthetic ^{14}C incorporation ($TO^{14}CP$), (b) gross primary production (GPP), (c) community respiration (DCR) and (d) net community production (NCP) in the Ría de Vigo. Black dots: position of *in situ* seawater sampling points for chemical and biological variables

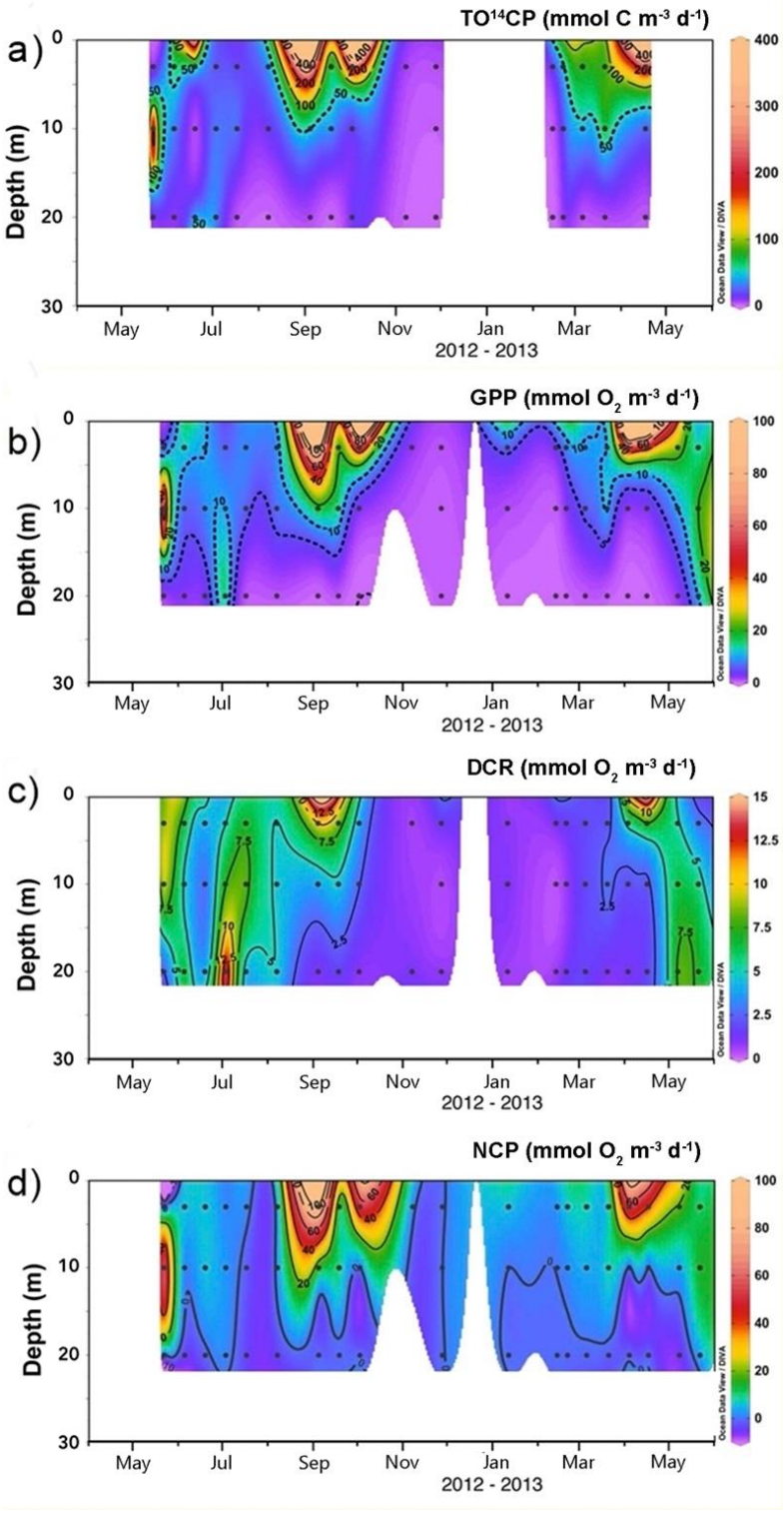

Fig. 6. Relationships between gross primary production (GPP) and chlorophyll *a* (chl *a*). Black, blue and red dots are data from 3, 10 and 20 m depth, respectively. Data points with a sampling date correspond to the sub-surface chlorophyll maximum (SCMs). Black dotted line: general relation including all data except the SCM outliers (GPP = 5.02[±0.19] × chl *a* – 4.11[±0.87]; R^2 = 0.93, p < 0.0001, n = 52). Continuous black, blue and red lines: relationships obtained with data from 3, 10 and 20 m depth, respectively; red dotted line: relationship including 20 m depth plus SCM data

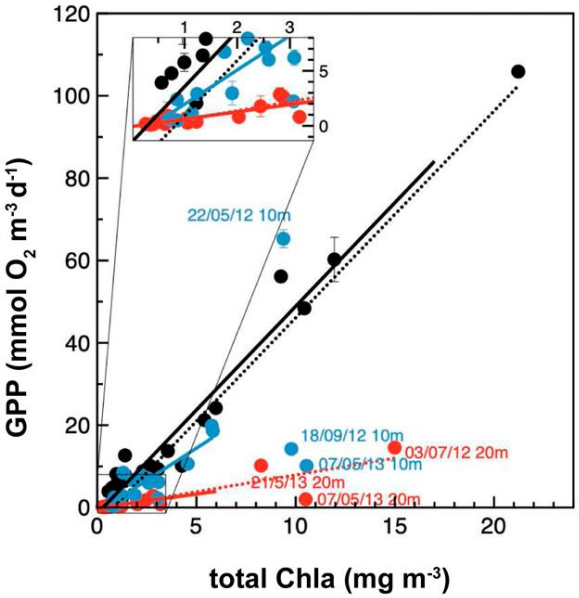

Fig. 7. Relationships of integrated community respiration (DCR) with integrated (a) gross primary production (GPP) and (b) total chlorophyll *a* (chl *a*). Red open squares: data from the late autumn + winter; blue crosses: spring; black circles: summer; black filled blue circles: early autumn (September–October 2012). Error bars: ±SE. Black thin line in (a) is the 1:1 line; blue lines in both graphs are the significant regression lines obtained with spring data. Sub-surface chlorophyll maximum data are marked with their sampling date and are excluded as outliers from the relationship in (a)

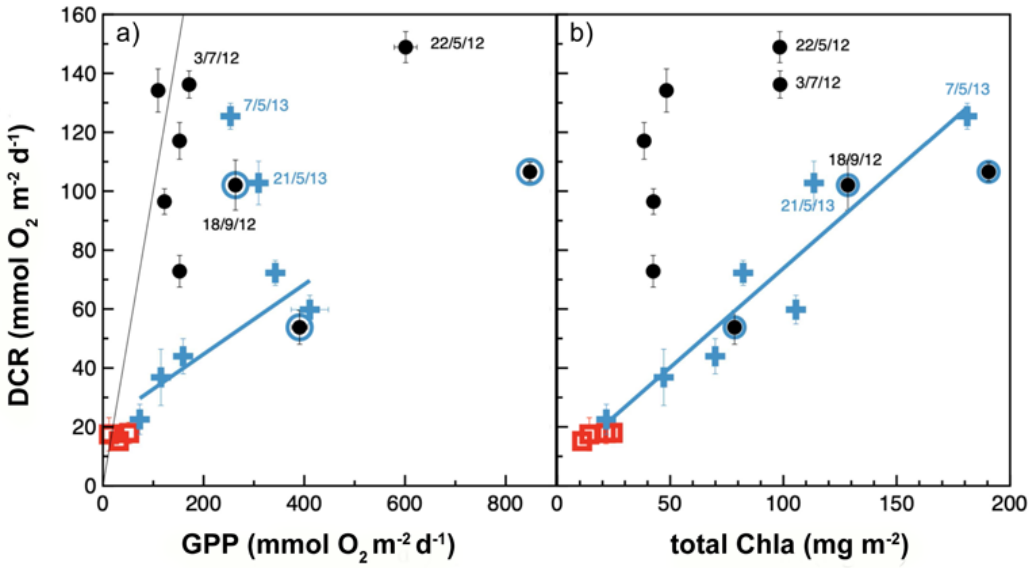

Fig. 8. Integrated gross primary production (GPP) to integrated total photosynthetic ^{14}C incorporation ($TO^{14}CP$) relationships. Black dots, blue crosses and red squares are data from summer + early autumn, spring and late autumn + winter, respectively. Data points with a sampling date correspond to the sub-surface chlorophyll maximum. Continuous black and blue lines are the regression lines obtained with data from early autumn–summer and spring, respectively

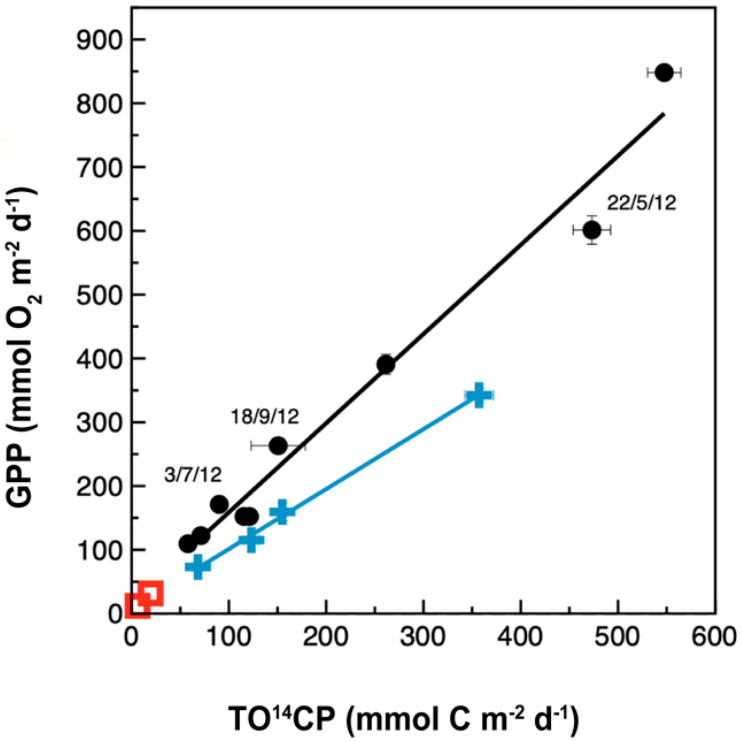

Fig. 9. Relationships of the integrated percentage of microphytoplankton (% chl $a_{>20\mu m}$) with (a) integrated community respiration (DCR), (b) integrated DCR:gross primary production (GPP) ratio, and (c) integrated DCR:chl *a* ratio. Red squares: data from the late autumn + winter; blue crosses: spring; black dots: summer + early autumn. Error bars: ±SE. Solid lines in (b) and (c) correspond to the regression lines obtained with summer + early autumn integrated data

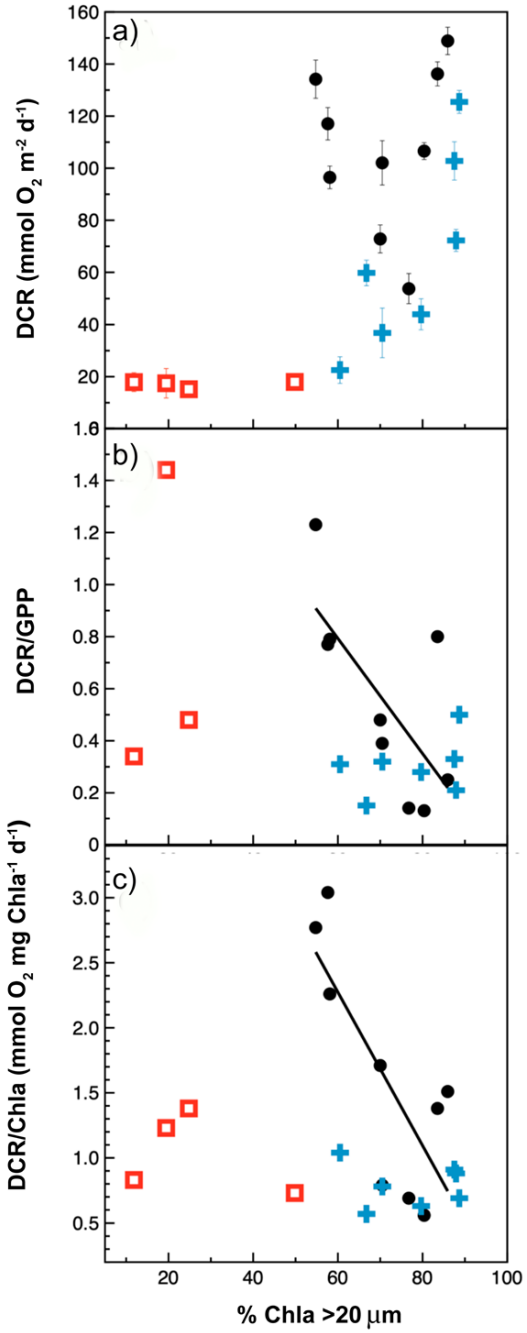

Fig. 10. Relationship between the GPP:DCR ratio vs. (chl $a_{>20\mu m}$:chl *a* total). Grey-black symbols are results from Arbones et al. (2008), corresponding to four 10 d surveys in the Ría de Vigo (Apr, Jul, Oct 2004 and Jan 2005), and one survey in Jul 2005 carried out in the shelf outside the Ría de Vigo (MAB). Orange dots, red open squares and blue crosses are our results of summer + early autumn, late autumn + winter and spring, respectively. Modified from Fig. 6b in Arbones et al. (2008)

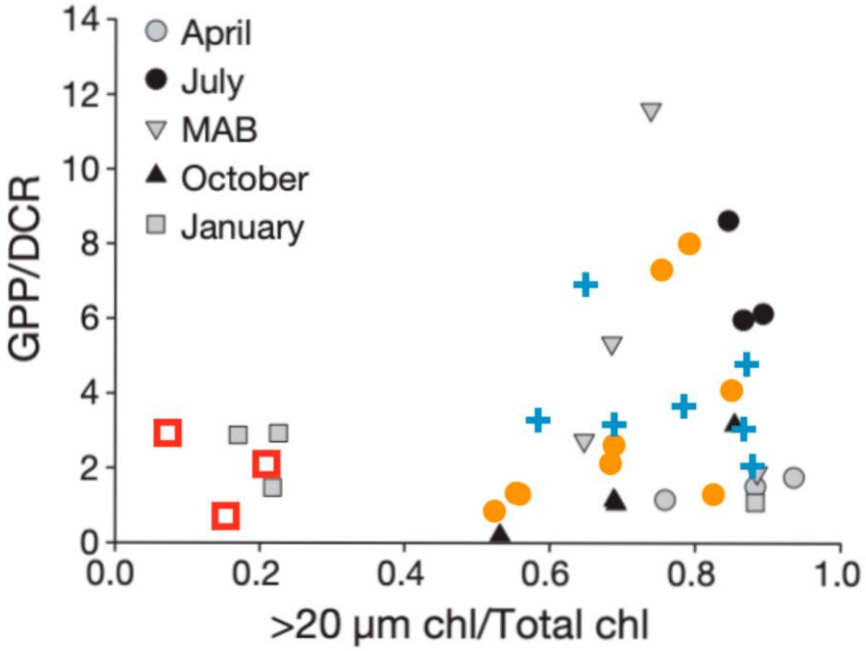

Fig. 11. Relationships between integrated net community production (NCP) and integrated total photosynthetic ^{14}C incorporation ($TO^{14}CP$). Dashed horizontal line: the zero line for NCP. Red open squares: data from the late autumn + winter; blue crosses: spring; black filled dots: summer + early autumn. Black continuous line: regression line obtained with summer and early autumn integrated data only (NCP = 1.38[±0.11] × $TO^{14}CP$ – 84.82[±32.41]; R^2 = 0.95, p < 0.0001, n = 9); dotted line: regression line obtained with winter- and spring-integrated data (NCP = 0.74[±0.02] × $TO^{14}CP$ – 4.76[±3.74]; R^2 = 0.99, p < 0.0001, n = 6). Error bars: ±SE